



HAL
open science

Nanoscale Evidence Unravels Microalgae Flocculation Mechanism Induced by Chitosan

Irem Demir, Jonas Blockx, Etienne Dague, Pascal Guiraud, Wim Thielemans, Koenraad Muylaert, Cécile Formosa-Dague

► **To cite this version:**

Irem Demir, Jonas Blockx, Etienne Dague, Pascal Guiraud, Wim Thielemans, et al.. Nanoscale Evidence Unravels Microalgae Flocculation Mechanism Induced by Chitosan. *ACS Applied Bio Materials*, 2020, 3 (12), pp.8446-8459. 10.1021/acsaabm.0c00772 . hal-03025212

HAL Id: hal-03025212

<https://laas.hal.science/hal-03025212>

Submitted on 26 Nov 2020

HAL is a multi-disciplinary open access archive for the deposit and dissemination of scientific research documents, whether they are published or not. The documents may come from teaching and research institutions in France or abroad, or from public or private research centers.

L'archive ouverte pluridisciplinaire **HAL**, est destinée au dépôt et à la diffusion de documents scientifiques de niveau recherche, publiés ou non, émanant des établissements d'enseignement et de recherche français ou étrangers, des laboratoires publics ou privés.

20 **ABSTRACT**

21 ~~In light of climate change, there is a growing interest for sustainable energy.~~ Microalgae are a
22 promising resource for biofuel production, although their industrial use is limited by the lack of
23 effective harvesting techniques. Flocculation consists in the aggregation and adhesion of cells into
24 flocs that can be more easily removed from water than individual cells. Although it is an efficient
25 harvesting technique, contamination is a major issue as chemical flocculants are often used. An
26 alternative is to use natural biopolymers flocculants, such as chitosan. Chitosan is a bio-based non-
27 toxic polymer, which has been effectively used to harvest *Chlorella vulgaris* cells at pH lower than its
28 pKa (6.5). While the flocculation mechanism reported relied on electrostatic interactions between
29 chitosan and the negative cell surface, no molecular evidence has yet confirmed this mechanism. In
30 this study, we performed force spectroscopy AFM experiments to probe the interactions between *C.*
31 *vulgaris* cells and chitosan at the molecular scale to decipher its flocculation mechanism. Our results
32 showed that at pH 6, chitosan interacts with *C. vulgaris* cell wall through biological interactions,
33 rather than electrostatic interactions. These observations were confirmed by comparing the data
34 with cationically modified cellulose nanocrystals, for which the flocculation mechanism, relying on an
35 electrostatic patch mechanism, has already been described for *C. vulgaris*. Further AFM experiments
36 also showed that a different mechanism was at play at higher pH, based on chitosan precipitation.
37 Thus this AFM-based approach highlights the complexity of chitosan-induced flocculation
38 mechanisms for *C. vulgaris*.

39

40

41

42

43

44

45 **KEYWORDS:** Atomic force microscopy, Force spectroscopy, Microalgae, Flocculation, Chitosan,
46 Cellulose nano-crystals

47 These last two decades, the global interest for microalgae has increased, notably because of
48 their oil production capacity that makes them an interesting alternative resource for biofuel
49 production.¹ Indeed, several studies have estimated that microalgae could produce between 40 000
50 and 90 000 L of biofuel per Ha, depending on the sunlight and the biomass oil content of the species
51 considered.²⁻⁴ This represents up to 200 times more liters than soybean and 25 times more liters
52 than oil palm.⁵ Among the wide variety of microalgae species, several have been considered for
53 biofuel production such as *Chlorella vulgaris*. *C. vulgaris* is a unicellular freshwater microalgae species
54 first discovered in 1890 by a Dutch researcher.⁶ This species first attracted attention in the 1950s for
55 its nutritional value, as its protein content represents up to 55% of its dry mass⁷. Nowadays, *C.*
56 *vulgaris* is mainly used for nutraceutical purposes; studies have shown for example that it has
57 immune-modulating and anti-cancer properties^{8,9}, but has also received interest for biofuel
58 production⁴. Indeed, *C. vulgaris* has the capacity to accumulate important amounts of lipids under
59 certain culture conditions, with a fatty acid profile adapted for biofuel production.^{7,10,11}

60 But presently, the commercialization of microalgae-based biofuels is hindered by the lack of
61 economically competitive harvesting techniques, as this step is generally estimated to represent 20-
62 30% of the total microalgal biomass production cost.^{12,13} In the case where the harvesting step is
63 combined with lipid extraction, as needed in biofuel production processes, this cost can increase up
64 to 90%, resulting in a negative energy balance for the production of microalgae-based biofuels at
65 large scale.¹⁴⁻¹⁶ The parameters that make harvesting microalgae such a challenging task are their
66 low concentration in water, their small cell size, their negatively charged surface, and their low
67 density. So far, different harvesting techniques have been proposed, including centrifugation,
68 filtration, flotation, flocculation, and electrical-based processes. A recent review compared and
69 described the advantages and disadvantages of each of these techniques.¹³ Among them,
70 flocculation stands out as it is inexpensive, making it an option for large-scale harvesting for a wide

71 variety of microalgae species.¹⁷ Flocculation consists in the aggregation of cells to facilitate their
72 separation from water by sedimentation or flotation for example. While this technique presents
73 many advantages, a major issue in flocculation is contamination, as it often requires the use of
74 chemical flocculants to induce flocculation, which end up in the harvested biomass, and can interfere
75 with downstream processes or with its final application.¹⁸ In this context, an interesting alternative is
76 to use biopolymers to induce flocculation¹⁹, the most popular in microalgae harvesting being
77 chitosan.

78 Chitosan is a cationic polyelectrolyte obtained by deacetylation of chitin, an abundant
79 natural polymer. Chitosan presents many advantages compared to traditional inorganic flocculants
80 as it is non-toxic, biodegradable, biocompatible, and renewable.^{20,21} Moreover, chitosan does not
81 contaminate the harvested biomass as chitin-like polysaccharides are naturally present in the cell
82 wall of many microalgae species, including *C. vulgaris*, and thus harvested cells can then be directly
83 exploited.²² Chitosan-induced flocculation has so far been used to harvest successfully both fresh-
84 water and marine microalgae species. For fresh-water species such as *C. vulgaris*, its efficiency is
85 mostly attributed to the amino groups present in chitosan. These groups have a pKa value of about
86 6.5²³, and thus below this pH these groups are mostly protonated and confer a positive charge to
87 chitosan, which allows supposedly its electrostatic interaction with the negatively charged surface of
88 microalgae cells.²⁴ As a result, cells are believed to be flocculated through a charge neutralization
89 mechanism.²⁵⁻²⁷ In the case of marine microalgae species, mixed results on chitosan efficiency have
90 been reported. Indeed, at the high ionic strengths of marine waters, it is believed that the positives
91 charges of chitosan are shielded, preventing further flocculation through charge neutralization.
92 However some studies reported successful flocculation of certain marine species by chitosan²⁸⁻³¹,
93 which may suggest that chitosan-induced flocculation may rely on different interactions between
94 chitosan and cells than electrostatic interactions. In this view, an interesting paper from 2011
95 focused on the influence of the cell wall carbohydrate composition of *C. vulgaris* on the efficiency of
96 chitosan-induced flocculation.³² The results obtained in this study show that a higher polysaccharide

97 content (including neutral sugars, uronic acids and amino sugars) in the cell wall is associated with a
98 better efficiency of flocculation with chitosan at high pH (8.5), suggesting that non-electrostatic
99 absorption of chitosan on cells may be more important than electrostatic neutralization in *C.*
100 *vulgaris*. However, in all the reported cases of flocculation of *C. vulgaris* using chitosan as a
101 flocculant, no molecular evidences has been provided, so that the mechanism(s) underlying the
102 flocculation remains unclear.

103 In this study, we investigated the interactions between chitosan and *C. vulgaris* cells using an
104 advanced technique: atomic force microscopy (AFM). AFM, first developed in 1986³³, is a highly
105 sensitive force machine able to record forces as small as 20 pN, making it possible to gain insights
106 into the molecular interactions between single living cells and their environment. Our team recently
107 used AFM to understand the flocculation mechanism involved in the cases of three different
108 microalgae species, demonstrating the interest of using this technology to answer such questions.^{34–}
109 ³⁶ Thanks to AFM force spectroscopy experiments, we show for the first time that at pH 6 below its
110 pKa, chitosan interacts with *C. vulgaris* cell wall through non-electrostatic interactions, *i. e.* through
111 specific interactions between chitosan and polymers at the surface of cells that are being unfolded
112 upon retraction. These observations were confirmed by comparing the data obtained with
113 cationically modified cellulose nanocrystals (CNCs), for which the flocculation mechanism, relying on
114 an electrostatic patch mechanisms, has been suggested in a previous study from our team on *C.*
115 *vulgaris*.³⁷ Further AFM experiments, including force spectroscopy but also roughness analysis,
116 however showed that at higher pH, the mechanism at play is different, as chitosan is not able to
117 interact with cells at such high pH. Thus our AFM-based approach allows in this study to highlight the
118 complexity of chitosan-induced flocculation in the case of *C. vulgaris*, and enabled us to identify, at
119 pH 6, a new flocculation mechanism based on the biological binding of chitosan with the cell wall of
120 cells. Given the wide use of chitosan in microalgae harvesting processes, these new data provide
121 important information to optimize microalgae-based biofuel production.

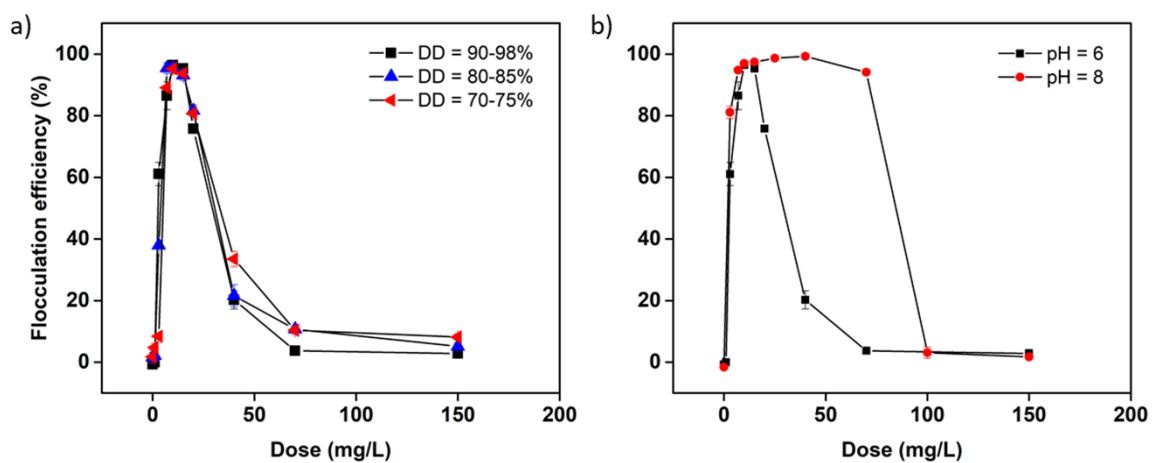
122

123 RESULTS AND DISCUSSION

124 Macroscopic observations show that chitosan does not interact electrostatically with cells

125 In a previous work where we evaluated the efficiency of cationically-modified CNCs to
126 flocculate *C. vulgaris* cells, we showed that the number of positive charges present on the CNCs was
127 directly correlated with the flocculation efficiency.³⁷ Indeed, CNCs bearing more positive charges
128 allowed more efficient flocculation compared to CNCs with less positive charges. This was explained
129 by the fact that positive CNCs interact with cells through electrostatic interactions, and thus the more
130 positive charges present, the more interactions can occur with cells, resulting in a higher flocculation
131 efficiency. Based on the literature, this situation should be similar for chitosan at a pH of 6, so below
132 the pKa value of the amine groups of chitosan. To test this hypothesis, we performed flocculation
133 experiments using different chitosan molecules with different degrees of deacetylation (DD), thus
134 bearing more or less positive charges. The DD of each chitosan was determined using
135 conductometric titration and established to be of $77.5 \pm 0.8\%$, $80.5 \pm 1.4\%$ and $85.2 \pm 0.2\%$ (see
136 Figure S1 and Table S1). The dynamic viscosity of the chitosan stock solutions (5 g/L in 0.04 M HCl)
137 was measured under different shear stress (see Table S2). Chitosan in solution acts as a non-
138 newtonian liquid: increasing shear stress reduces the dynamic viscosity. The results obtained for the
139 flocculation experiments are presented in figure 1a. They show that surprisingly, the flocculation
140 efficiency is similar for all chitosans tested, with a maximum efficiency reached for a dose of 10 mg/L,
141 thus showing that there is no influence of the DD of chitosan, and thus of its number of positive
142 charges on the flocculation of cells. This in line with the work of Chen *et al.*, who also showed that
143 the DD of chitosan had indeed a limited impact on the flocculation of bentonite.³⁸ Moreover, this
144 study also showed that the molecular weight of chitosan had a dominant influence on the
145 flocculation efficiency, with high molecular weights allowing to reach higher flocculation efficiencies.
146 In our case, the MW of the chitosan that was used is of 345.2 kDa, thus high, which explains perhaps
147 the high efficiencies reached in our flocculation experiments (> 95%). To verify this observation, we
148 compared the flocculation efficiencies with a pH of 8 where chitosan does not present positive

149 charges. In this case, if the flocculation efficiency of chitosan is based on electrostatic interactions,
 150 then no flocculation should be observed at this higher pH environment. However, the results
 151 obtained, presented in Figure 1b, show that a maximum flocculation efficiency can be reached for
 152 the same chitosan dose both at pH 6 and 8. While this efficiency drops at higher doses for a pH of 6,
 153 it remains maximum for doses up to 80 mg/L for a pH of 8. This result can be correlated to previous
 154 data obtained in our team for the marine species *Nannochloropsis oculata* where it was shown that
 155 chitosan was efficient even when used at higher pH conditions.³¹ It was showed that at higher pH,
 156 the uncharged chitosan precipitates causing the flocculation of the cells through a sweeping
 157 mechanism where cells are mechanically trapped in the massive structure of the precipitate³⁹,
 158 instead of charge neutralization as it is supposed to be the case at pH 6. Overall the flocculation
 159 results presented here seem not to be in accordance with the literature, and comfort the idea,
 160 previously raised in 2011 in the case of *C. vulgaris*³², that the interactions between cells and chitosan



161 may not rely on electrostatic interactions.

162 **Figure 1: Flocculation experiments of *C. vulgaris* with chitosan.** Flocculation efficiency of a) different
 163 chitosan molecules with different deacetylation degree (DD) at pH 6 and b) chitosan molecules with
 164 DD = 77.5 ± 0.8% at pH 6 and 8.

165

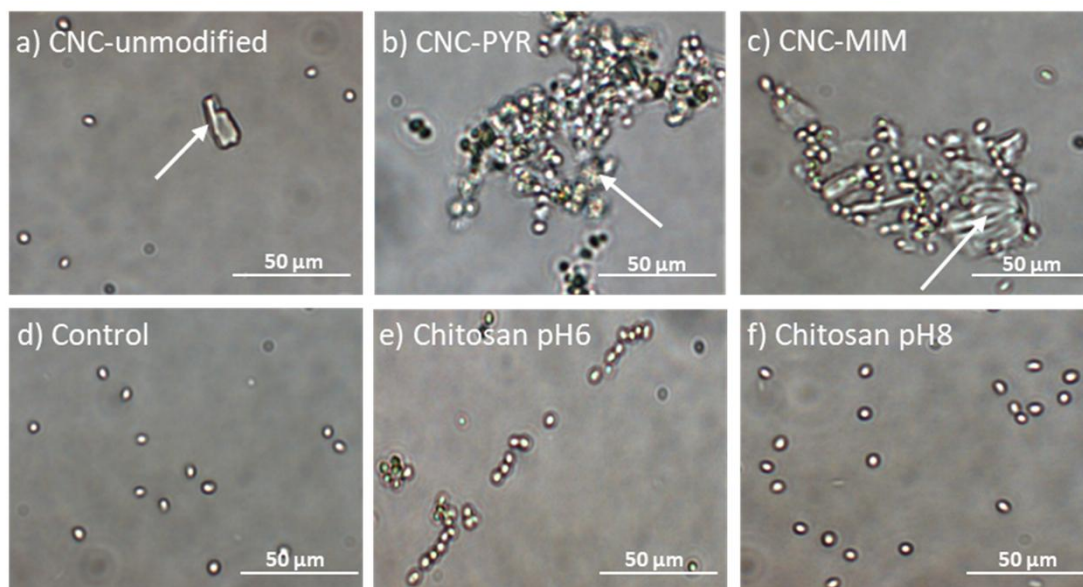
166 To understand this phenomena further, we performed an optical microscopy assay with cells
 167 incubated with CNCs and chitosan used at concentrations for which the best flocculation efficiencies
 168 were obtained (10 mg/mL for chitosan and 100 mg/L for CNCs³⁷). For chitosan, we chose to work

169 with the chitosan with a degree of deacetylation of $77.5 \pm 0.8\%$ (4.2 mmol charges/g). Three types of
170 CNCs were used in this study: unmodified CNCs, CNCs modified with pyridinium grafts (CNC-PYR, DS =
171 0.20, 0.92 mmol charges/g) and CNCs modified with methylimidazolium grafts (CNC-MIM, DS = 0.23,
172 0.99 mmol charges/g). The used CNCs were fully characterized in a previous study by the authors.³⁷
173 Both CNC-PYR and CNC-MIM have quaternary ammonium groups which carry a permanent positive
174 charge independent of pH, unlike chitosan, for which the charge carried by its primary amines are
175 only charged after protonation at low pH.^{37,40} The results are presented in Figure 2. When CNCs were
176 used, CNCs particles can directly be observed on the images (indicated by arrows): in the case of
177 unmodified CNCs (Figure 2a), no cells are attached to the particles, while for CNC-PYR and CNC-MIM,
178 cells aggregated around the particles could be observed (Figure 2b and c). This is then coherent with
179 the patch mechanism already described for *C. vulgaris* in our previous work where cells interact
180 electrostatically with CNC particles. Thus, in the case of unmodified CNCs that do not have positive
181 charges, no interactions with cells could be observed. However for chitosan, the situation is different:
182 at pH 6, small aggregates of cells were observed, with smaller size than the CNC aggregates (Figure
183 2e), suggesting that chitosan does interact with cells, but that perhaps the nature of the bond is
184 different, not as strong as in the case of CNCs. At pH 8, cells do not seem to be aggregated (Figure
185 2f). If we follow the hypothesis formulated in our previous work on *N. occulata*³¹, then this results
186 could be explained by the fact that at higher pH, the flocculation mechanism is based on sweeping,
187 and thus there are no direct interactions between chitosan and cells. This is also in line with what
188 was already demonstrated on another microalgae species, *Dunaliella salina*; when sweeping
189 mechanism is involved, there are no interactions between the flocculant and the cells.³⁵ Thus, at this
190 stage, our macroscopic analysis seems to show that in contrast to the literature, chitosan-induced
191 flocculation in *C. vulgaris* may not rely on electrostatic interactions, even at pH 6 where chitosan is
192 positively charged. However, what is then the mechanism involved?

193

194

195
196
197
198
199
200



201 **Figure 2. Optical imaging of *C. vulgaris* flocculation.** Optical image of *C. vulgaris* cells after
202 resuspension in PBS containing a) 100 mg/L of CNC-unmodified at pH 8, b) 100 mg/L of CNC-PYR at
203 pH 8, c) 100 mg/L of CNC-MIM at pH 8, d) nothing at pH 6, e) 10 mg/L of chitosan at pH 6, and f) 10
204 mg/L of chitosan at pH 8. The arrows in a), b) and c) indicate the CNC particles.

205

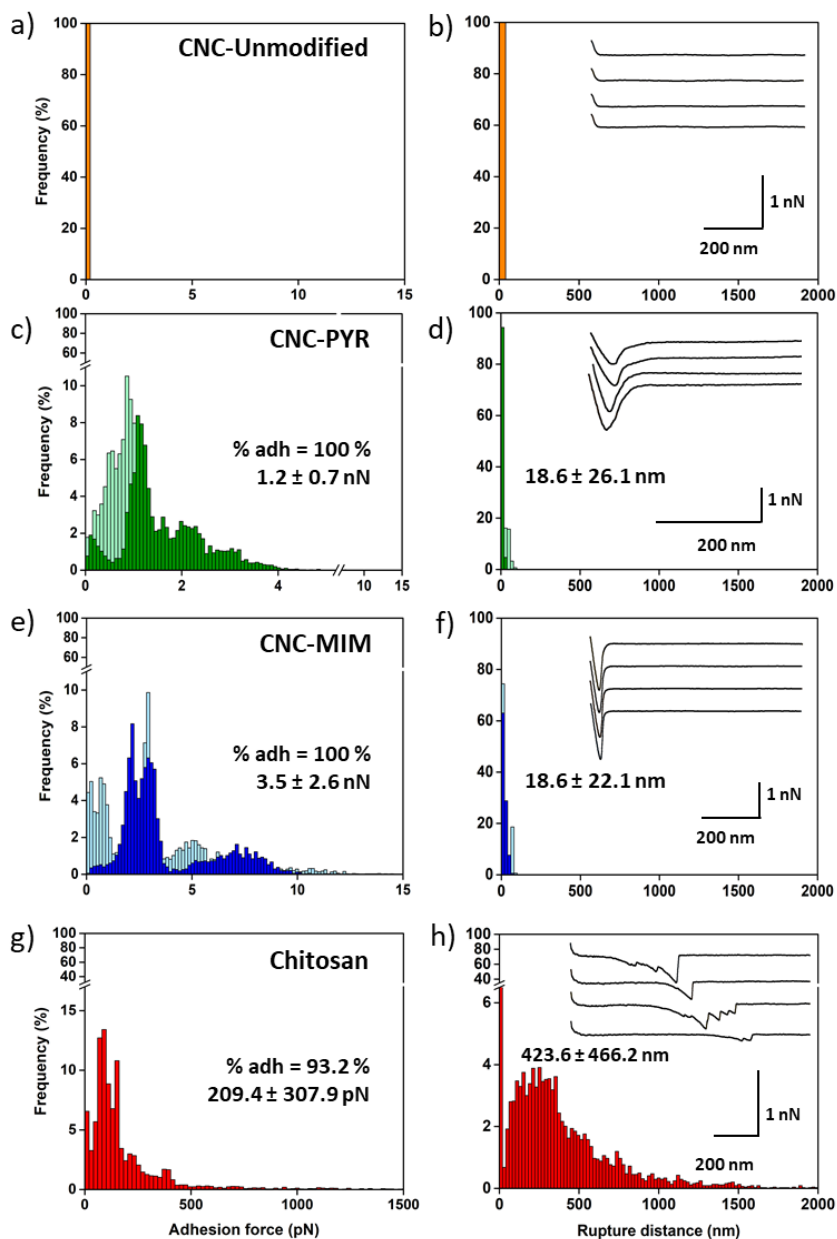
206 **AFM nanoscale scale experiments reveal the role of biological interactions between cells and** 207 **chitosan during flocculation**

208 To answer this question, we used atomic force microscopy (AFM) in order to directly probe
209 the interactions between the flocculants and cells and to get a better insight into the flocculation
210 mechanisms involved in each case. We first performed force spectroscopy experiments to probe the
211 interactions between CNCs and single *C. vulgaris* cells. For that, a first method (method 1 described
212 in the Methods section, Figure S2a) has consisted in using tips directly modified with CNCs (Figure S3)
213 to probe the interactions with cells immobilized on a positive glass surface at a pH of 8. In the case of

214 CNCs, the charge present on the particles is not dependent on the pH because the modified CNCs
215 carry a quaternary ammonium group that is permanently positively charged. But because this first
216 method was difficult to implement for modified CNCs, as the forces recorded between the CNCs
217 particles and cells were stronger than the electrostatic forces between the cells and the surface on
218 which they were immobilized, only a small number of cells could be probed. Indeed, during force
219 spectroscopy, the cells would detach from the surface to adhere to the CNC particle on the probe,
220 therefore making the measurements impossible. To overcome this challenge, we also recorded data
221 using FluidFM technology (method 2 in the Methods section, Figure S2b). In this case, single cells
222 were aspirated at the aperture of microfluidic probes by exerting a negative pressure inside the
223 cantilever microchannel. This negative pressure was sufficient to keep the cells attached to the
224 cantilever, and thus more measurements could be performed. The data presented in Figure 3
225 combines data obtained with these two methods for modified CNCs (details of these data can be
226 found in Table S3); in the case of unmodified CNCs, only the first method was used. In this figure, the
227 adhesion forces, rupture distances and representative force curves recorded in PBS buffer are
228 presented. The adhesion force corresponds to the strongest adhesion event in each force curve,
229 while the rupture length is the distance of the last adhesion event recorded. The percentage of
230 adhesion indicated corresponds to the percentage of force curves presenting retract adhesions. In
231 each case, the results presented correspond to the interactions recorded with 10 cells coming from
232 at least 2 independent cultures. In the case of unmodified CNCs (Figure 3a and b), and in line with
233 our previous work, no interactions with cells can be observed, as retract force curves show no retract
234 peaks. In the case of CNC-PYR (Figure 3c and d), a single retract peak happening at the contact point
235 can be observed, with in this case an average force of 1.2 ± 0.7 nN ($n = 9801$ force curves). This force
236 signature is typical of non-specific interactions, most likely reflecting electrostatic interactions
237 between the negative surface of the cells and the positive surface of PYR-modified CNCs.³⁴ Similar
238 force curves could be obtained for CNCs-MIM (Figure 3e and f), however, in this case the average
239 adhesion force recorded was of 3.5 ± 2.6 nN ($n = 8845$ force curves), so almost 3 times higher than

240 for CNCs-MIM. The adhesion force difference between CNC-MIM and PYR is significant at a p-value of
241 0.001 (unpaired t-test). This is an interesting point; indeed, CNC-MIM have a higher number of
242 positive charges compared to CNC-PYR, and our results indicate that this difference influence the
243 adhesion force recorded. Thus the more positive charges on the CNCs are present, the stronger the
244 electrostatic bond with the cell's surface is. However, the difference in DS between both cationic
245 CNCs is small (CNCs-PYR, DS = 0.20 and CNCs-MIM, DS = 0.23), not fully explaining the big differences
246 in adhesion forces. An explanation for these differences might reside in the chemical structure of the
247 cationic grafts on the CNCs. In the CNC-PYR sample, the cationic charge is distributed over a 6-
248 membered ring, while only over a 5-membered ring in the CNC-MIM sample, causing different charge
249 densities at the atomic level. Moreover methylimidazolium has two nitrogen atoms in its ring
250 structure, while pyridinium only contains one; this could also contribute to the difference recorded in
251 the adhesion forces. Regarding the rupture distance recorded, they were in average of 18.6 ± 26.1
252 nm for CNC-PYR, and of 18.6 ± 22.1 nm for CNC-MIM, indicating that no molecules were pulled away
253 from the surface of the cells. Thus, these results confirmed that the interactions between cationic
254 CNCs and cells are non-specific and electrostatic. Hence, this molecular data confirms that in the case
255 of CNCs-induced flocculation a charge neutralization mechanism is involved, and it explains why
256 better flocculation efficiencies are obtained using CNCs bearing a higher number of positive charges.
257 To further prove this point, and exclude possible contributions of other types of interactions
258 between CNCs and cells, additional experiments were carried out to measure the interactions
259 between beads bearing COOH functionalities, thus negatively charged at a pH of 8, and CNCs
260 immobilized on mica surfaces. These beads have a similar size to the cells, and thus are here used as
261 artificial non-living analogues of microalgae cells bearing only negative charges and no surface
262 polymers. The results (Figure S4) show the same tendency, *i. e.* single peak retract force curves and
263 lower adhesion values obtained with CNCs-PYR (5.3 ± 1.4 nN, n = 800 force curves obtained with 2
264 different beads), compared to CNCs-MIM (49.6 ± 10.6 nN, n = 800 force curves obtained with 2
265 different beads). In this case, the adhesion values are higher than the ones obtained with cells; this

266 can be explained by the fact that the beads were more negatively charged than cells. Indeed, zeta
 267 potential measurements have shown that at a pH of 8, cells have a surface potential of -21.9 mV,
 268 whereas the zeta potential of beads is of -43.2 mV.



269
 270 **Figure 3. Interactions between CNCs or chitosan and single *C. vulgaris* cells.** a) Adhesion force
 271 histogram between *C. vulgaris* cells and CNCs-unmodified at pH 8 and b) corresponding rupture
 272 distance histogram. c) Adhesion force histogram between *C. vulgaris* cells and CNCs-MIM at pH 8
 273 and d) corresponding rupture distance histogram. The light green distributions correspond to values
 274 obtained with method 1 and the dark green distributions correspond to values obtained with method
 275 2. e) Adhesion force histogram between *C. vulgaris* cells and CNCs-MIM at pH 8 and f) corresponding
 276 rupture distance histogram. The light blue distributions correspond to values obtained with method
 277 1 and the dark blue distributions correspond to values obtained with method 2. g) Adhesion force
 278 histogram between *C. vulgaris* cells and chitosan spin-coated on a glass slide at pH 6 and h)

279 corresponding rupture distance histogram. Insets in b), d), f) and h) show representative force curves
280 obtained. Data were recorded using a set-point of 0.25 nN.

281

282 However, the interesting result from these force spectroscopy analysis concerns chitosan

283 (Figure 3g and h). In this case, the interactions between a single living *C. vulgaris* cell immobilized at

284 the edge of a tipless cantilever⁴¹, and a chitosan-functionalized surface by spin-coating^{42,43} were

285 probed at a pH of 6 (method 3 in the Methods section, Figure S2c). In this case, retraction force

286 profiles showed multiple binding events with an average adhesion force of 209.4 ± 307.9 pN ($n =$

287 5698 force curves), thus much lower than the forces recorded for cationic CNCs. In contrast, the

288 average rupture length for chitosan was 423.3 ± 466.2 nm, whereas in the case of cell interactions

289 with CNCs it was close to zero. Note that the large standard deviations come from the wide

290 distributions of the values visible on the histograms, caused by the heterogeneity inherent to living

291 cells. The extended ruptures, the low adhesion forces recorded, as well as the lack of defined force

292 patterns are consistent with the stretching of long molecules from the cell wall of cells.⁴⁴⁻⁴⁶ Given the

293 difference in the force signatures obtained, our results suggest that in the case of chitosan, even

294 when positively charged, no electrostatic interactions are involved in the bonding with cells, or at

295 least if electrostatic interactions are involved they are not predominant in the interactions and are

296 masked by the biological interactions. This inherently implies that chitosan is able to interact

297 specifically with polymers present at the surface of cells that are then unfolded upon retraction in

298 our force spectroscopy experiments, resulting in the long rupture distances observed. Taking into

299 account the work of Cheng and coworkers, who showed that the carbohydrate composition of the

300 cell wall of *C. vulgaris* has a direct influence on the efficiency of flocculation obtained with chitosan³²,

301 we may suggest that chitosan is able to specifically interact with these polysaccharides. Moreover,

302 similar force patterns were already observed for microalgae by Higgins and coworkers who extended

303 mucilage (composed of polysaccharides) from the cell wall of *Craspedostauros australis*, a marine

304 diatom, and of *Pinnularia viridis*, a freshwater diatom⁴⁷. This further supports that the unfolding

305 observed in our case may be due to the unfolding of polysaccharides from the *C. vulgaris* cell wall.

306 For the moment, such specific structural interactions between chitosan and polysaccharides, not

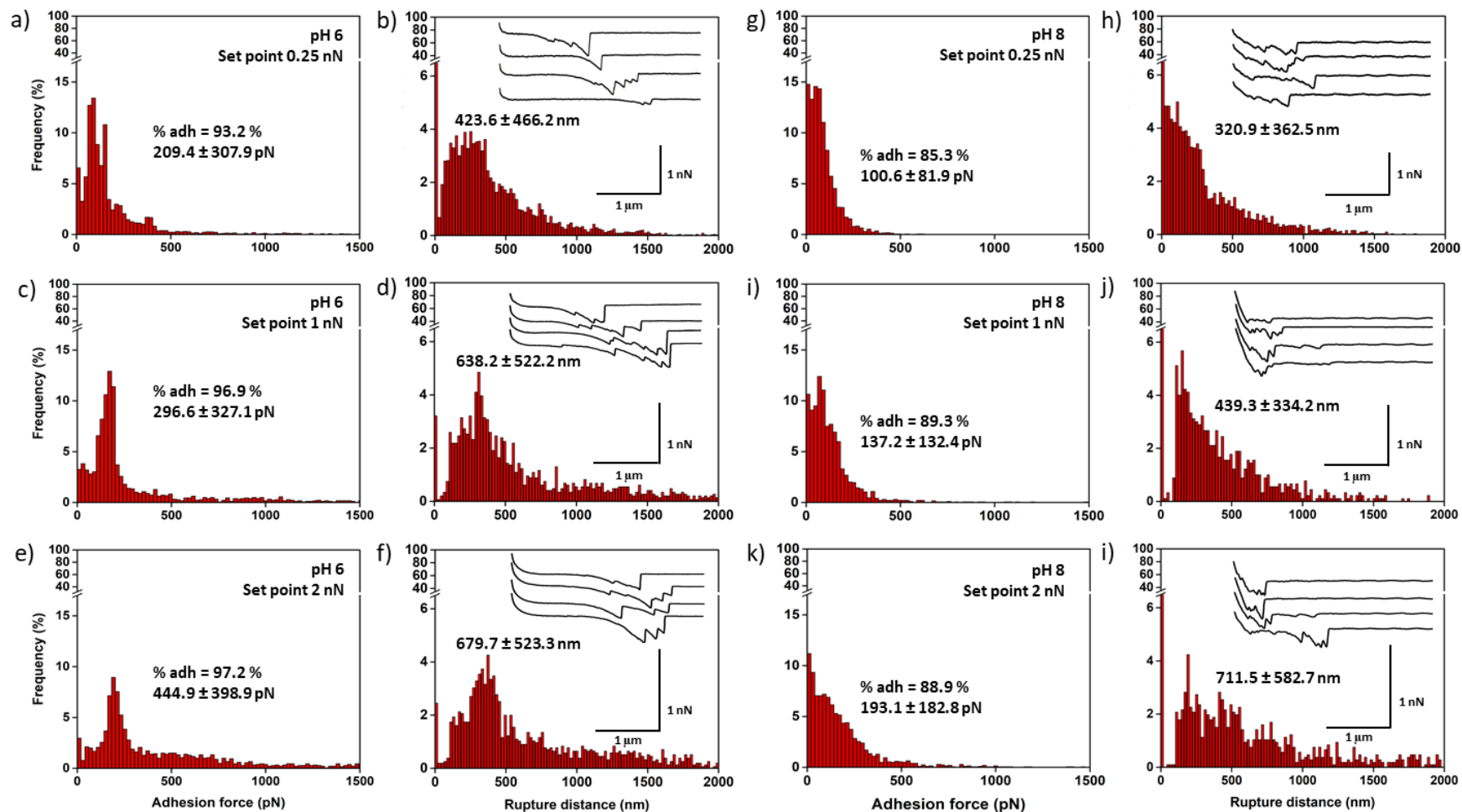
307 dependent on electrostatic interactions, have been described only in a few cases, for example with
308 cellulose⁴⁸ or with alginate,⁴⁹ for which interactions with chitosan have been observed at high or low
309 pH, where either the polysaccharides or the chitosan are uncharged. Moreover, previous studies
310 have also reported the possible interaction between chitosan and glycopolymers in the case of
311 microorganism flocculation: for example Barany *et al.* showed that *Escherichia coli* flocculation by
312 chitosan relied on chitosan absorption to polymers from the cells, rather than on electrostatic
313 factors.⁵⁰ Thus, at this stage, the data obtained indicate that chitosan flocculation at pH 6 in the case
314 of *C. vulgaris* does not occur through electrostatic interactions, but rather through biological
315 interactions, meaning that chitosan interacts with biomolecules at the cell surface that are then
316 unfolded from the cell surface. These biomolecules might be polysaccharides present at the surface
317 of the cells. More questions can now be raised: can further data prove this? Is this mechanism also at
318 play at pH 8?

319

320 **Chitosan induced-flocculation of *C. vulgaris* at higher pH does not occur through the same** 321 **mechanism**

322 To further investigate the flocculation mechanism of chitosan, we decided to compare the
323 interactions between chitosan and cells at pH 6 and 8 at varying applied forces. When the applied
324 force is increased during force spectroscopy experiments, because the chitosan layers are
325 deformable (Y_m of 15.6 ± 30.5 kPa at pH 6, $n=1554$ force curves, and of 19.2 ± 23.2 kPa at pH 8,
326 $n=1349$ force curves, values extracted from force curves at an indentation segment of 100 nm, data
327 not showed), the contact area between the cells and the chitosan surface increases as well. This
328 increase should lead to higher adhesion forces as more molecules from the cell wall are able to
329 interact with the chitosan surface; rupture lengths will also provide useful information on the nature
330 of the molecules unfolded. The results of these experiments are presented in Figure 4, they were
331 obtained in the case of a set point of 0.25 nN with 10 different cells, and in the case of higher set
332 points with 4 different cells coming from at least 2 independent cultures (details of the data can be

333 found in Table S3, S4 and S5). In each case, the differences between the adhesion forces recorded at
334 pH 6 and pH 8, for the different set-points, are significantly different at a p-value of 0.001 (unpaired
335 t-test). At pH 6, we can observe that the more the applied force was increased, the more the average
336 adhesion force increased, from 209.4 ± 307.9 pN at an applied force of 0.25 nN (Figure 4a, $n = 5698$
337 force curves), to 296.6 ± 327.1 pN at 1 nN (Figure 4c, $n = 2050$ force curves) and 444.9 ± 398.9 pN at
338 2 nN (Figure 4e, $n = 2050$ force curves), thus two times higher. As for the rupture distances, they also
339 increase with the applied force, from in average 423.6 ± 466.2 nm at 0.25 nN (Figure 4b) up to 679.7
340 ± 523.3 nm at 2 nN (Figure 4f). This thus indicates that as the contact surface area increases between
341 the cell and the chitosan surface, the more molecules, probably polysaccharides, from the cell wall
342 involved in the interactions with chitosan were extended, resulting in higher adhesion forces and
343 rupture distances. When these experiments were performed at a pH of 8, a similar trend was
344 observed, with an increase in both the maximum adhesion force and rupture length when the
345 applied force is higher. However, an interesting point to note in this case is the difference in values
346 between the measurements performed at pH 6 and pH 8. Indeed, in the case of pH 8, the average
347 adhesion force recorded was 193.1 ± 182.8 pN at an applied force of 2 nN (Figure 4k, $n = 2050$ force
348 curves), thus almost equivalent to the adhesion force recorded at pH 6 for the smallest applied force
349 (0.25 nN). Regarding rupture lengths, although the average distances recorded were similar at a high
350 force applied, their difference is important at a low applied force (423.6 ± 466.2 nm at pH 6 and
351 320.9 ± 362.5 nm at pH 8). The differences in these values are surprising as one would expect that if
352 the interaction mechanism is indeed based on biological interactions, the same molecules would
353 unfold from the cell surface irrespective of the pH, resulting in similar unfoldings with similar rupture
354 distances. These results thus seem to indicate that it is not the case.



355
356
357
358
359
360

Figure 4. Interaction between chitosan and single *C. vulgaris* cells at pH 6 and 8 at varying applied forces. a) Adhesion force histogram and b) corresponding rupture distance histogram between a *C. vulgaris* cell-functionalized cantilever and chitosan spin-coated on a glass slide at pH 6 using a set-point of 0.25 nN, c) and d) using a set-point of 1 nN, e) and f) using a set-point of 2 nN. g) Adhesion force histogram and h) rupture distance histogram between a *C. vulgaris* cell-functionalized cantilever and chitosan spin-coated on a glass slide at pH 8 using a set-point of 0.25 nN, i) and j) using a set-point of 1 nN, k) and l) using a set-point of 2 nN. Insets in b), d), f), h), j) and l) show representative force curves obtained.

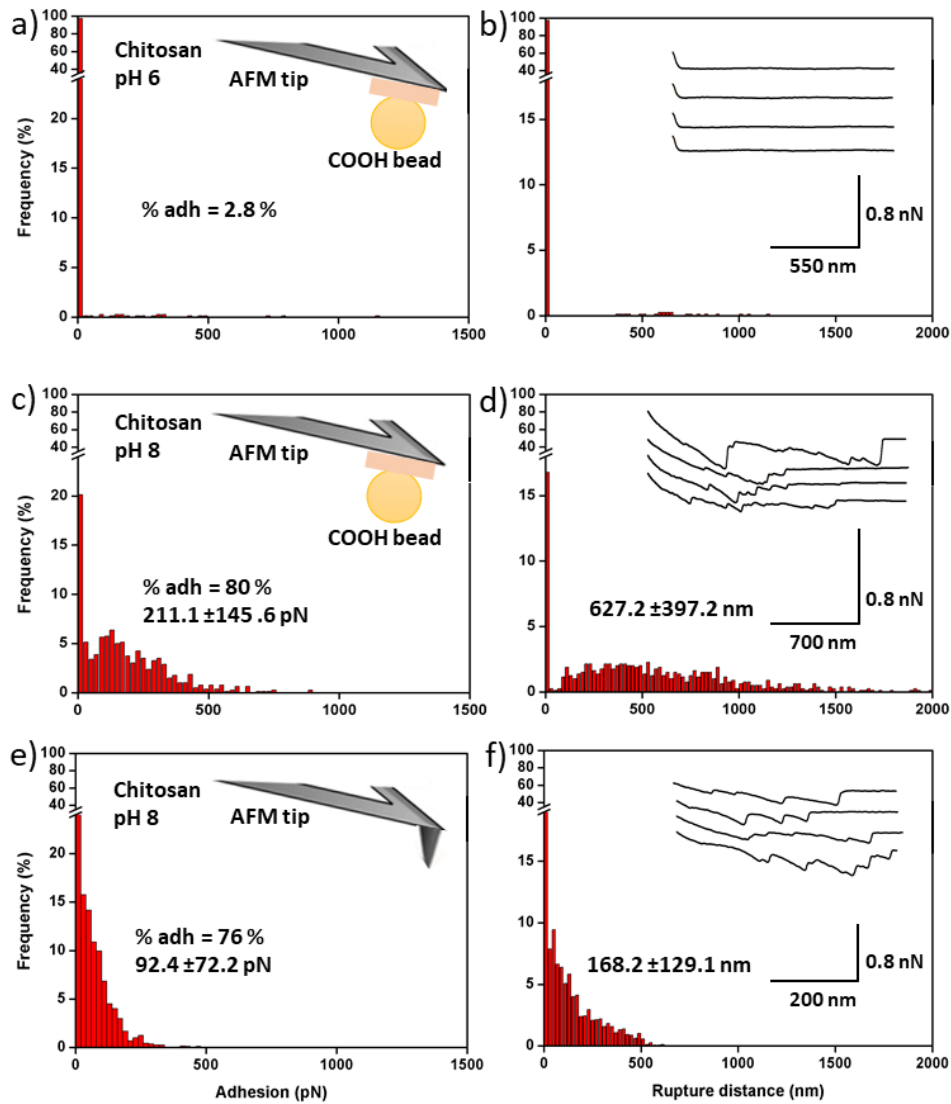
361 To understand this behavior, we performed experiments with negatively charged beads, and
362 probed the interactions with chitosan surfaces at pH 6 and 8. The results are presented in Figure 5.
363 At pH 6, few interactions were recorded between the beads and the chitosan surface (2.8 % of the
364 force curves), as most retract force curves present no retract peaks (Figure 5a and b). This thus
365 proves our first hypothesis that chitosan interactions with cells do not rely dominantly on
366 electrostatic interactions but on biological interactions. Indeed, COOH beads enables us to mimic the
367 cell surface by bearing negative charges, but have the advantage to exclude the molecules that are
368 present on the cell walls. In this case, it is clear that the biological polymers that are present on the
369 microalgal cell surface are essential for the interaction of chitosan with the cell, and that the charge
370 of chitosan is not dominant in the interaction with cells in our experimental conditions. Moreover, as
371 for experiments where the interactions between cells and chitosan were probed at pH 6 (Figure 4),
372 no electrostatic interactions were recorded. This further indicates that these interactions, either do
373 not take place or are smaller than the limit of detection of AFM (20 pN), and thus cannot be
374 captured. This is an interesting point because at pH 6 chitosan is positively charged, and should in
375 theory interact with negatively charged surfaces; thus perhaps these interactions are too weak to be
376 detected. The poor strength of electrostatic interactions between positively charged chitosan at low
377 pH and negative surfaces has already been described in other research fields. For example, chitosan
378 has been used to bind with negatively charged drugs in order to form drug loaded chitosan nano- and
379 microparticles.⁵¹ However it is showed in several studies that the release of the drugs from chitosan
380 particles is rapid, indicating that the binding properties of chitosan through electrostatic interactions
381 may be poor.⁵¹

382

383

384

385



386 **Figure 5. Interaction between bare tips and negative beads-functionalized cantilevers with**
 387 **chitosan surfaces.** a) Adhesion force histogram between a COOH bead-functionalized cantilever and
 388 chitosan spin-coated on a glass slide at pH 6 and b) corresponding rupture distance histogram. c)
 389 Adhesion force histogram between a COOH bead-functionalized cantilever and chitosan spin-coated
 390 on a glass slide at pH 8 and d) corresponding rupture distance histogram. e) Adhesion force
 391 histogram between a bare AFM tip chitosan spin-coated on a glass slide at pH 8 and f) corresponding
 392 rupture distance histogram. Insets in b) d) and f) show representative force curves obtained. Data
 393 were recorded using a set-point of 0.25 nN.
 394

395 When the same experiments are performed at a pH of 8 (Figure 5c and d), force curves show
 396 multiple peaks that have a similar profile to the ones obtained using cells instead of beads, with
 397 average adhesion forces and rupture lengths recorded values of 211.1 ± 145.6 pN and 627.2 ± 397.2
 398 nm ($n = 800$ force curves, with 2 different beads), respectively. Using bare tips instead of beads
 399 (Figure 5e and f), the same unfolding events were recorded, with similar adhesion and rupture

400 distances values as in the case of cells. This result is unexpected: indeed, the bare tips used, as for
401 the beads, carried no polymers, *i.e.* the multipeaks observed on the force curves must correspond to
402 the unfolding of chitosan picked up directly from the surface upon retraction by the tips or the
403 beads. This indicates that at this pH, the structure of chitosan must be different than at pH 6 where
404 bare tips do not allow the unfolding of chitosan. Moreover, this gives the explanation for the results
405 obtained using living cells at pH 8 (Figure 4g-l): in this case also, the chitosan must be unfolded from
406 the surface which explains why the adhesion forces and rupture lengths values obtained are different
407 from those obtained at pH 6. Given the fact that the same chitosan unfoldings were obtained with
408 cells, negative beads or bare tips, we can thus conclude that at pH 8 there is no biological nor
409 electrostatic interaction between the cells and chitosan, in agreement with the optical images
410 obtained (Figure 2e) where no cell aggregation could be visualized. The fact that higher adhesions
411 and rupture lengths values are recorded with beads compared to cells or bare AFM tips is explained
412 by the fact that the surface contact with beads is larger (6-7 μm of diameter compared to 3-4 μm of
413 diameter for cells), thus allowing the AFM tip to pull more chitosan from the surface. The
414 flocculation mechanism of cells at pH 8 is thus based on a different mechanism than at pH 6; our
415 hypothesis is that at this pH, the chitosan precipitates and flocculates the cells by sweeping, as we
416 have demonstrated in our previous study.³¹ We now need to verify this hypothesis.

417

418 **Sweeping mechanism is involved in the flocculation of *C. vulgaris* at pH 8**

419 The previous results have demonstrated that cells do not interact through biological or
420 electrostatic interactions with chitosan at pH 8. However, the question is now to understand if this is
421 due to changes in the cell wall properties of the cells, to changes in the chitosan structure, or to
422 both? It has been shown previously with the marine species *Phaeodactylum tricornutum* that the cell
423 wall rigidity changed with pH, which impacted on the deformability of the cells and thus on their
424 interactions with their environment.³⁴ Moreover, AFM studies on microorganisms have shown that
425 under some conditions, the architecture and network of molecules at the surface of cells can change

426 depending on the external conditions, which thus impacts on the availability of molecules to interact
427 with their environment.⁴⁵ To verify these two points in our study, we performed nanomechanical
428 analysis of the cell wall of cells as well as surface roughness analysis. These results are presented in
429 Figure 6. To obtain quantitative information on the nanomechanical properties of the cells, we
430 determined the Young modulus (Y_m) of the microalgae cells through nanoindentation measurements,
431 in PBS at pH 6 and pH 8 (Figure 6a and b). In this type of measurements, the cantilever, for which
432 mechanical properties are known, is pressed against the cells at a given force. This enables us to
433 extract the Y_m of the cell wall, a parameter that reflects its resistance to compression (the higher the
434 Young modulus value, the more rigid the cell wall). Nanoindentation measurements, which give
435 access to force vs distance curves, were performed on areas of $500 \text{ nm} \times 500 \text{ nm}$ on top of cells, on 8
436 cells coming from at least 2 independent cultures. Y_m values were then obtained first by converting
437 the force curves obtained into force vs indentation curves, shown in Figure 6a, and then by fitting
438 them with a theoretical model, in our case, the Hertz model⁵² (black empty circles on the curves in
439 Figure 6a). The results show that the indentation curves obtained on cells at pH 6 and 8 are different;
440 indeed, the AFM probe is able to indent deeper into cells at pH 6 than at pH 8, meaning that
441 increasing the pH also increases the rigidity of the cell wall. Quantitative analysis of the Y_m extracted
442 from thousands of these curves on 8 cells in each case confirmed this finding, and showed that at pH
443 6, cells have an average Y_m of $232.9 \pm 175.6 \text{ kPa}$ ($n = 8192$ force curves), whereas cells at pH 8 have a
444 Y_m of $750.2 \pm 589.0 \text{ kPa}$ ($n = 8182$ curves, differences are significant at a p-value of 0.001, unpaired t-
445 test, details can be found in table S6). While the nanomechanical properties of *C. vulgaris* have never
446 been determined using AFM before, these values are in the range of Y_m values obtained on other
447 microorganisms such as yeasts, that have a cell wall composition comparable to microalgae.⁵³
448 Moreover, this increase in the rigidity, due to the increase of pH, has already been shown in the case
449 of *P. tricornutum*.³⁴ Hence, increasing the pH changes the nanomechanical properties of the cell wall
450 and thus its architecture, perhaps explaining in part the fact that cells are not able to interact with
451 chitosan at pH 8. Indeed, it could mean that the molecules involved in the interaction with chitosan

452 are not available anymore for interaction, or that their conformation at elevated pH prevents the
453 interaction with chitosan. Regarding the cell wall roughness, this parameter was directly extracted
454 from contact images of 500 nm × 500 nm obtained on top of 8 cells coming from at least 2
455 independent cultures. The results obtained (Figure 6c-f) show that the surface morphology is slightly
456 modified by the increase in pH, as shown by the vertical deflection images recorded on top of the
457 cells in Figure 6c and d. Cross-sections taken along the white lines in Figure 6c and d show this
458 difference, as the profile of this cross-section at pH 8 presents larger motives. The quantitative
459 analysis of the roughness measured on several cells showed that at pH 6, cells have an average
460 roughness of 0.9 ± 0.5 nm while it increased to 1.7 ± 0.9 nm at pH 8. While this difference is
461 significant, it remains low and indicates that at pH 8, more molecules protrude from the surface of
462 the cell, which might mask the molecules involved in the interaction with chitosan, or perhaps might
463 indicate that these molecules are coiled and not able to interact anymore.⁴⁵ Overall this biophysical
464 analysis of the cell wall of *C. vulgaris* indicates that a pH increase from 6 to 8 clearly affects its rigidity
465 and its roughness. These changes, as discussed, may explain why cells do not interact with chitosan
466 anymore at pH 8.

467

468

469

470

471

472

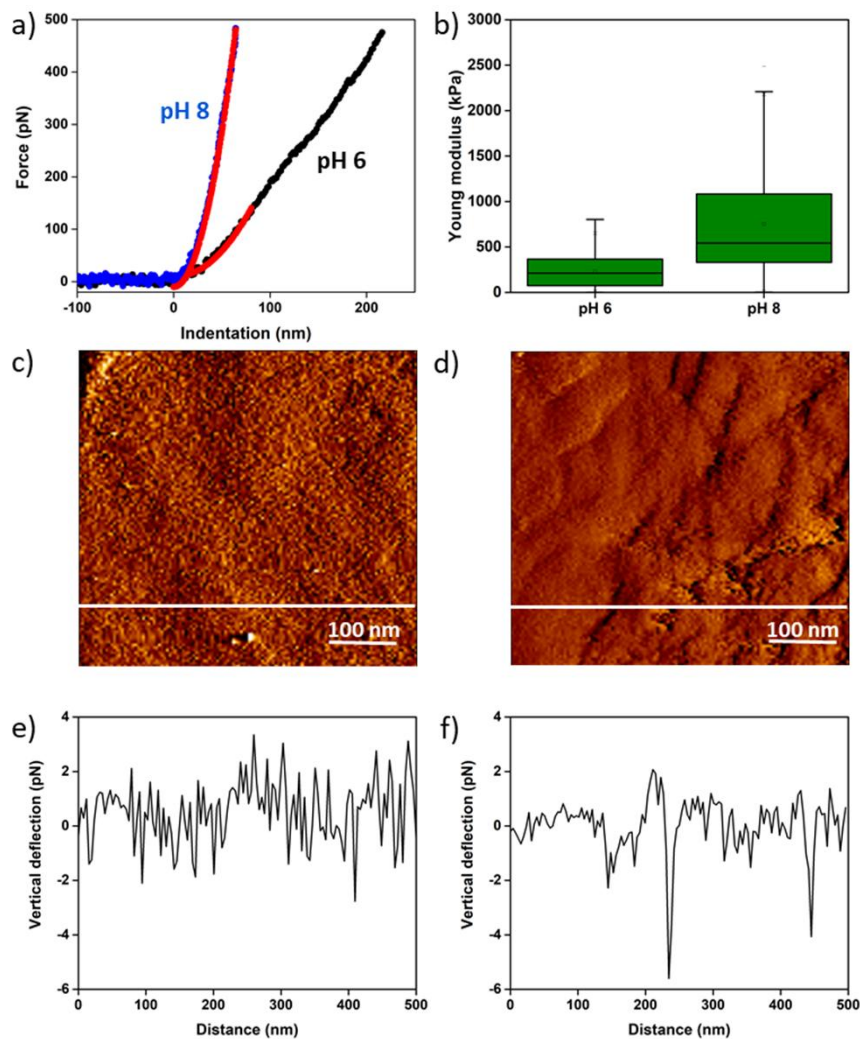
473

474

475

476

477

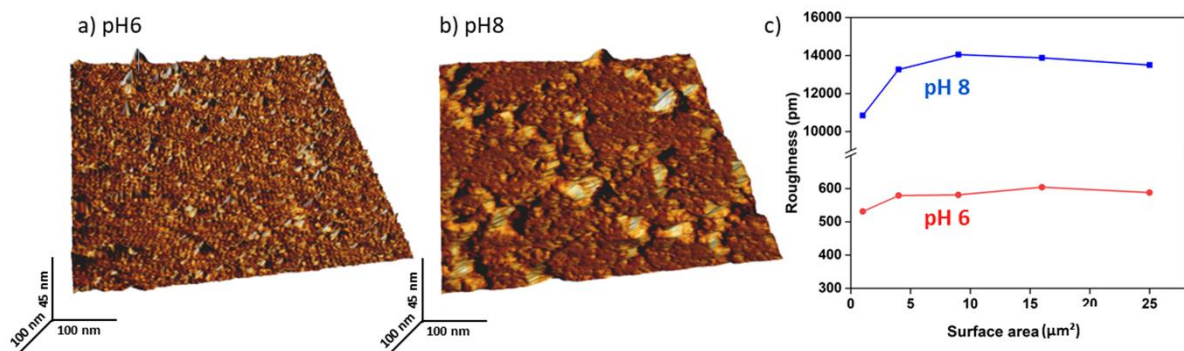


479

480 **Figure 6. Nanomechanics and cell wall roughness of the *C. vulgaris* cell wall.** a) Indentation curves
 481 (blue and black lines) fitted with the Hertz model at 80 nm of indentation (red lines) recorded on top
 482 of *C. vulgaris* cells at pH 6 and 8. b) Boxplot of the Young's modulus values measured on top of *C.*
 483 *vulgaris* cells at pH 6 and 8. c) Vertical deflection AFM image of an area (500 × 500 nm) of the cell
 484 surface at pH 6 and d) vertical deflection AFM image of an area (500 × 500 nm) of the cell surface at
 485 pH 8. e) Cross-section taken along the white line in c) and f) cross-section taken along the white line
 486 in d).
 487

488 To determine if this lack of interactions is also due to the chitosan itself, we also performed
 489 roughness measurement on the chitosan functionalized surfaces used in all the experiments. The
 490 results, presented in Figure 7, showed an average roughness of chitosan of 0.6 ± 0.1 nm at a pH of 6,
 491 which increased dramatically, to 13 ± 5 nm at a pH of 8. This result indicates that the pH has an
 492 important effect on the structure of the chitosan, which, precipitates and gets detached from the

493 surface. This detachment from the surface creates aggregates of chitosan, as it can be seen on the
494 height image recorded (Figure 7b), which leads to an important roughness. This explains why
495 chitosan can be pulled out from the surface in force spectroscopy experiments, whatever the probe
496 used (cell, negatively charged bead, or bare AFM tip). This precipitation might lead to a decrease of
497 its specific surface available for interaction, which can also be a rational explanation to the fact that
498 cells do not interact with chitosan at pH 8. Thus, from these experiments, we can conclude that the
499 fact that chitosan does not interact with the cell wall of *C. vulgaris* at pH 8 results from the
500 combination of changes associated directly with the structure of the cell wall with changes in the



501 structure of chitosan itself caused by its precipitation.

502 **Figure 7. Characterization of chitosan surfaces at two different pH.** a) 3D AFM height image of
503 chitosan surface at pH 6. b) 3D AFM height image of chitosan surface at pH 8. c) Quantification of
504 chitosan surface roughness at pH 6 and 8.
505

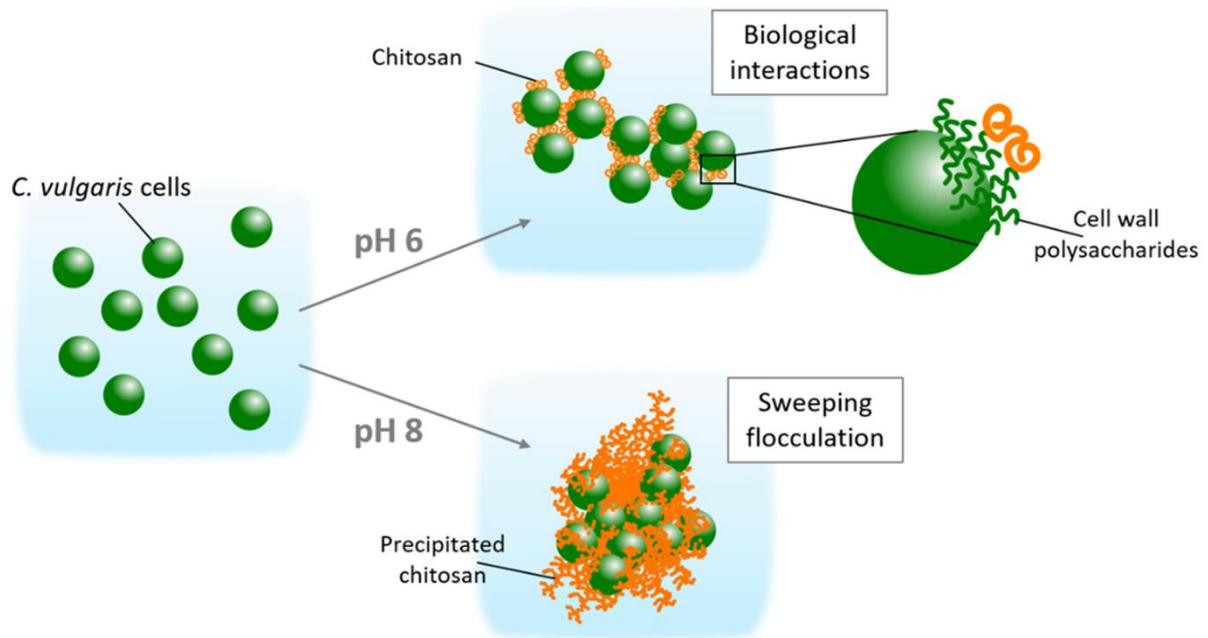
506 CONCLUSION

507 Chitosan, given its many advantages, has been widely used as a flocculant to efficiently
508 harvest diverse species of microalgae. Since understanding the flocculation mechanisms is key to
509 control them and use them in larger-scale processes, the case of chitosan has generated a lot of
510 debate in the scientific community. Indeed, while for freshwater species that grow at pH below 6.5,
511 chitosan-induced flocculation is believed to rely on a charge neutralization mechanism, some studies
512 also show it becomes more efficient at higher pH, while in marine waters were the salts present
513 screen the charges of chitosan, chitosan can still flocculate microalgae. It is therefore of great
514 importance to provide new data, using original techniques, to finally shed light on the flocculation

515 mechanism at play. For that we have chosen the freshwater green species, *C. vulgaris*, and studied at
516 the nanoscale its interactions with chitosan using atomic force microscopy. Our results demonstrate
517 that depending on the pH, the interaction mechanism is different, which reveals the complexity of
518 chitosan flocculation. Indeed, preliminary macroscopic observations suggest that the charge of
519 chitosan is not involved in the interaction with cells, as different degrees of deacetylation result in
520 the same flocculation efficiency at pH 6. At increased pH, for the same degree of deacetylation, the
521 flocculation behavior is different as high doses of chitosan still allow an efficient separation, which is
522 not the case at pH 6. Based on these observations, our force spectroscopy experiments show that at
523 pH 6, chitosan interacts in a specific way with most probably polysaccharides present on the surface
524 of cells, and that the chitosan charge is not significantly involved in these interactions. This was
525 confirmed by comparing these data with those obtained for cationically modified CNCs, for which a
526 previous study has demonstrated the contribution of only of charge neutralization in the flocculation
527 mechanism.³⁷ However, such biological interactions between chitosan and the surface of cells could
528 not be detected at pH 8. Indeed, biophysical analysis of the cell wall of *C. vulgaris* cells, as well as
529 roughness analysis of the chitosan used in this study suggest that at this pH, both the architecture of
530 the cell wall and the structure of chitosan are modified, resulting in an absence of interactions with
531 the cells. Based on a previous work published last year where we had found that a sweeping
532 mechanism is involved in the chitosan-induced flocculation of *N. oculata* at high pH, we thus suggest
533 that this mechanism is also at play for the flocculation of *C. vulgaris* at high pH. These different
534 mechanisms of flocculation are depicted in Figure 8. This study thus represents an original
535 contribution to the field of microalgae harvesting as molecular-scale data allow in this case to
536 understand the flocculation mechanisms and to show the important influence of the culture medium
537 pH on these mechanisms. Therefore, this work brings important information that will help in
538 implementing chitosan-induced flocculation to harvest microalgae at large-scale. Further work is now
539 needed to identify the polymers from the cell surface that interact specifically with chitosan at pH 6.
540 Because a large amount of microalgae species share the same surface characteristics, in particular

541 the composition, this knowledge would make it then be possible to perform efficient chitosan
542 flocculation with a wide range of microalgae species.

543



544

545 **Figure 8. Schematic representation of the flocculation mechanisms induced by chitosan at pH 6 and**
546 **8 for *C. vulgaris*.**

547

548

549 METHODS

550 **Microalgae cultivation.** The green freshwater microalgae *Chlorella vulgaris* strain CCAP 211/11B
551 (Culture Collection of Algae and Protozoa) was cultivated in sterile conditions in Wright's cryptophyte
552 (WC) medium prepared in deionized water, adjusted to a pH of 7.8.⁵⁴ Cells were cultivated at 20°C,
553 under agitation (120 rpm), in 1L Erlenmeyer (300 mL of culture) flasks. The incubator was equipped
554 with white neon light tubes providing illumination of approximately 40 $\mu\text{mol photons m}^{-2} \text{ s}^{-1}$ with a
555 photoperiod of 18h light: 6h dark. All experiments were carried out with exponential phase batch
556 cultures (day 7).

557 **Cationically-modified cellulose nanocrystals (CNCs) synthesis.** N-Benzylmethylimidazolium Grafted
558 CNCs ([Br][Bnlm]-g-CNCs, referred in the text as CNCs-MIM) and Benzylpyridinium Grafted CNCs

559 ([Br][BnPy]-g-CNCs, referred in the text as CNCs-PYR), were synthesized and characterized in a
560 previous study and described in Blockx *et al.*³⁷ For the CNCs-MIM, the sample with a degree of
561 substitution (DS) of 0.23 was used, whereas for the CNCs-PYR, the sample with a DS of 0.20 was used.

562 **Chitosan.** Three different types of chitosan were used in this study. Commercial chitosan was
563 purchased from Sigma Aldrich (from shrimp, practical grade, $\geq 75\%$ degree of deacetylation (DD)). In
564 an earlier study it was determined that this chitosan has a M_n and M_w of 151.3 and 345.2 kDa
565 respectively, and a polydispersity of 2.28³¹. This chitosan was used throughout the paper for the
566 flocculation experiments and all AFM experiments. For flocculation experiments, two chitosan
567 samples with different DD (labelled as 70-75% and 80-85%) were prepared from shrimp shells and
568 kindly provided by Nha trang University, Vietnam. Chitosan stock solutions were produced by
569 dissolving 5 g/L of the three types of chitosan in 0.04 M of HCl, while stirring (1000 rpm) at ambient
570 conditions for 2 hours. A more exact degree of deacetylation was determined for the three chitosan
571 samples via conductometric titrations (Metrohm 856 Conductivity Module and 801 Stirrer with
572 TiamoTM software). For that, 2 mL stock solution was diluted 50 fold in MiliQ water and titrated with
573 5.75 mM NaOH under constant stirring. The results are shown in supplementary Figure S1 and Table
574 S1. The DD was determined from the volume of NaOH required to neutralize the chitosan (plateau
575 area of the curves), where each chitosan sample was measured three times. The DD of the
576 commercial Sigma Aldrich chitosan is of $77.5 \pm 0.8\%$, and for the chitosan samples provided by the
577 Nha trang University of $80.5 \pm 1.4\%$ and $85.2 \pm 0.2\%$. The dynamic viscosity of the three chitosan
578 samples was measured on a AR-G2 rheometer (TA Instruments) equipped with a steel double wall
579 couette cell. The experiment consisted of four steps. Step 1: 60 s at a shear rate of 100.0 /s to allow
580 the sample to set in the sample holder; Step 2: 180 s at a shear rate of 1.0 /s; Step 3: 180 s at a shear
581 rate of 10.0 /s; and Step 3: 180 s at a shear rate of 100.0 /s. All experiments were carried out at 25 °C
582 and 1 datapoint was collected per second. All samples were measured in triplicate. Data analysis was
583 performed with TA Instrument Trios Version 3.3.1.4364. The results are showed in Supplementary
584 Table S2.

585 **Flocculation experiments.** Flocculation of *C. vulgaris* was performed using standardized jar tests
586 experiments. The microalgae suspension was adjusted to a pH of 6 and the initial optical density (OD_i ,
587 $_{750\text{ nm}}$) was set at 0.7 (corresponding to 0.28 g/L). 50 mL tests samples were taken and intensively
588 stirred at 550 rpm to mix the suspension. Different concentrations of chitosan were then added (0, 1,
589 3, 7, 10, 15, 20, 40, 70, 150 mg/L) from the 5 g/L stock solutions and the suspensions were stirred at
590 200 rpm for 20 min to induce flocculation. The suspensions were subsequently decanted in falcon
591 tubes and allowed to settle for 30 min before measuring the optical density after settling (OD_f) of the
592 supernatant (at approximately 3 cm below the surface). The flocculation efficiency (η_a) was
593 calculated according to the following equation 1. For experiments at pH 8, the microalgae suspension
594 was adjusted to a pH of 8 priori to flocculation experiments and the chitosan concentrations used
595 were of 0, 3, 7, 10, 15, 25, 40, 70, 100, 150 mg/L.

$$\eta_a = \frac{OD_i - OD_f}{OD_i} \quad (1)$$

596

597 **Optical imaging experiments.** Flocculation was directly observed after resuspension of the cells in
598 Phosphate Buffer Saline (PBS) at a pH of 6 or 8 containing chitosan at a concentration of 10 mg/L or
599 CNCs-PYR or CNCs-MIM, both at a concentration of 100 mg/L. Flocculation levels were observed
600 using an Axio Observer Z1 microscope (Zeiss, Germany) at a magnification of 50x.

601 **Zeta potential experiments.** The global electrical properties of *C. vulgaris* cell surface as well as of
602 negative beads (COOH functionalized polystyrene beads diameter of 6.83 μm , Spherotech, USA) were
603 assessed by measuring the electrophoretic mobility with an automated laser zetameter (Zetasizer
604 NanoZS, Malvern Instruments). To this end, microalgae were harvested by centrifugation (3000 rpm,
605 3 min), washed two times in PBS at a pH of 6 or 8, and resuspended in the same solution at a final
606 concentration of 1.5×10^6 cell/mL. In the case of beads, they were first centrifuged (3 min, 13000
607 rpm) and washed two time in deionized water. For each condition, analysis was performed in
608 triplicate.

609 **AFM cantilever functionalization.** All AFM cantilever functionalizations were performed using a
610 Nanowizard III AFM (Bruker, USA), with triangular tipless NP-O10 probes (Bruker, USA, nominal
611 spring constant of 0.06 N/m and of 0.2 N/m).

612 Functionalization with CNCs: Colloidal probes were functionalized with cationic CNC particles.
613 Colloidal probes were obtained by attaching a single silica microsphere (5 μm of diameter, Bangs
614 Laboratories) with a thin layer of UV-curable glue (NOA 63, Norland Edmund Optics). These colloidal
615 probes were then put under UV-light for 10 min to allow the glue to cure. They were further dipped
616 into a thin layer of UV-curable glue, then into a thin layer CNCs particles deposited on a glass slide.
617 Functionalized cantilevers were then put under UV-light for 10 min to allow the glue to cure and
618 further characterized using scanning electron microscopy (Figure S3). The spring constant of the
619 colloidal probe was determined after attachment of the CNC particles using the thermal noise
620 method.⁵⁵

621 Functionalization with single *C. vulgaris* cells: AFM cantilevers were also functionalized with single *C.*
622 *vulgaris* cells grown during 7 days in the conditions described previously. For that, cantilevers were
623 first activated using oxygen plasma (3 min, 0.5 mbar) and then incubated in a 0.2% polyethylenimine
624 solution (PEI, Sigma-Aldrich) overnight. The AFM cantilevers were then rinsed in PBS at a pH of 6 or 8,
625 brought into contact with an isolated cell and retracted to attach it. Proper attachment of the cell on
626 the colloidal probe was checked using optical microscopy. The spring constant of the AFM cantilever
627 was determined prior to cell immobilization using the thermal noise method.⁵⁵

628 Functionalization with negatively charged beads: AFM cantilevers were functionalized using COOH
629 polystyrene beads (negatively charged at pH 6 and 8, diameter of 6.83 μm , Spherotech, USA). Beads
630 were first centrifuged (3 min, 13000 rpm) and washed two time in deionized water. A drop from this
631 solution was then deposited on a glass slide and allowed to dry at 37°C during 2 hours. Cantilevers
632 were first dipped into a thin layer of UV-curable glue (NOA 63, Norland Edmund Optics), and then
633 brought into contact a single isolated bead on the glass slide and retracted to attach it.
634 Functionalized cantilevers were then put under UV-light for 10 min to allow the glue to cure; proper

635 attachment of the COOH bead on the colloidal probe was checked using optical microscopy. The
636 spring constant of the COOH probe was determined after attachment of the COOH bead using the
637 thermal noise method.⁵⁵

638 **Force spectroscopy experiments.** Force spectroscopy experiments were conducted either by
639 functionalizing the cantilever with CNCs and probing the interactions with immobilized cells on a
640 surface (method 1), using FluidFM technology to aspirate a single *C. vulgaris* cell at the aperture of a
641 microfluidic AFM probe to probe interactions with cationic CNCs functionalized on a surface (method
642 2), or by functionalizing the AFM cantilever with a single *C. vulgaris* cells and probing the interactions
643 with chitosan immobilized on a surface (method 3). In each case, experiments were performed in PBS
644 at a pH of 6 or 8, using a NanoWizard III AFM (Bruker, USA). These 3 methods are also depicted in
645 Figure S2.

646 Method 1: This method was used to probe the interactions between CNCs or negatively charged
647 beads, and single *C. vulgaris* cells. In this case, CNCs (unmodified, PYR and MIM) or negatively
648 charged beads functionalized cantilevers were directly used to probe the interactions with *C. vulgaris*
649 cells immobilized on polyethylenimine (PEI Sigma P3143) coated glass slides prepared as previously
650 described⁵⁶. For that, cells were first harvested by centrifugation (3000 rpm, 3 min) and washed two
651 times in PBS at pH 6 or 8. Freshly oxygen activated glass slides were covered by a 0.2% PEI solution in
652 deionized water and left for incubation overnight. Then the glass slides were rinsed with deionized
653 water and dried under nitrogen. A total of 1 mL of the cell suspension was then deposited on the PEI
654 slides, allowed to stand for 30 min at room temperature, and rinsed with PBS at pH 6 or 8.

655 Method 2: This method was also used to probe the interactions between CNCs and single *C. vulgaris*
656 cells. As the forces recorded between CNCs and cells were stronger than the electrostatic forces
657 between PEI coated glass-slides and cells, this method was alternatively used to complete the data
658 sets. In this case, FluidFM technology was used (Cytosurge AG, Switzerland): this system connects the
659 AFM to a pressure pump unit and a pressure controller through a microfluidic tubing system.
660 Micropipette probes with an aperture of 4 μm (spring constant of 0.3 N/m) were used (Cytosurge AG,

661 Switzerland). First, PBS at a pH 8 was filled in the probe reservoir and was pressed through the
662 cantilever by applying an overpressure (100 mBar). The probe was then immersed in PBS and
663 calibrated using the thermal noise method prior to measurement. A single *C. vulgaris* cell was then
664 picked up from the surface of the Petri dish by approaching the FluidFM probe and applying a
665 negative pressure (−80 mBar). The transfer of the cell on the probe was verified by optical
666 microscopy. The cell probe was then used to probe the interactions with CNCs-functionalized mica
667 surfaces. For that, CNCs solutions at a concentration of 5 g/L were first sonicated for at least for 5
668 min, then deposited on mica surfaces and left for incubation overnight. After that the mica surfaces
669 were rinsed using PBS at pH 8 and taped at the bottom of the Petri dish used for the AFM
670 experiment.

671 Method 3: This method was used to probe the interactions between chitosan and single *C. vulgaris*
672 cells. In this case, AFM cantilevers functionalized with a single *C. vulgaris* cells were used to probe the
673 interactions with chitosan-functionalized surfaces, in PBS pH 6 or 8. Chitosan was functionalized at
674 the surface of glass-slide using spin-coating method, according to procedures described in ^{42,43}.
675 Briefly, 50 mg of chitosan was first dissolved in 10 mL of deionized water containing 30-50 μ L of
676 hydrochloric acid (HCl). This solution was then deposited on a clean glass slide and spin-coated at
677 1000 rpm for 3 min. The glass slides were then dried in an incubator at 50°C overnight, before use.

678 **Roughness analyses.** Roughness analyses were performed on cells immobilized on PEI-coated glass
679 slides and on chitosan-functionalized glass slides. In both cases, images were recorded in PBS at pH 6
680 or 8 using contact mode on a Nanowizard III AFM (Bruker, USA), with MSCT cantilevers (Bruker,
681 nominal spring constant of 0.01 N/m). Images were recorded using an applied force of < 0.5 nN. The
682 cantilevers spring constants were determined by the thermal noise method.⁵⁵

683 **Nanomechanical analysis.** For nanoindentation experiments, the applied force was comprised
684 between 0.5 and 2 nN depending on the condition with MSCT cantilevers (Bruker, nominal spring
685 constant of 0.01 N/m). Young's moduli were then calculated from 80 nm indentation curves using the
686 Hertz model⁵² in which the force F , indentation (δ) and Young's modulus (Y_m) follow equation 2,

687 where α is the tip opening angle (17.5°), and ν the Poisson ratio (arbitrarily assumed to be 0.5). The
688 cantilevers spring constants were determined by the thermal noise method.⁵⁵

$$F = \frac{2 \times Ym \times \tan \alpha}{\pi \times (1 - \nu^2) \times \delta^2} \quad (2)$$

689

690 **Scanning electron microscopy imaging of AFM cantilevers.** AFM cantilevers functionalized or not
691 with CNCs or chitosan were first carbonated and then imaged using a Jeol 6400 electron microscope
692 (Jeol, Tokyo, Japan) equipped with an EDS Bruker SDD detector, at an acceleration voltage of 20kV.

693

694 **ACKNOWLEDGEMENTS**

695 C. F.-D. is a researcher at CNRS. C. F.-D. acknowledges financial support for this work from the
696 Agence Nationale de la Recherche, JCJC project FLOTALG (ANR-18-CE43-0001-01). J. B., W. T. and K.
697 M. acknowledge financial support for this work from Research Foundation Flanders (grant
698 *G.0608.16N*) and from the EU Interreg France-Wallonie-Vlaanderen program through the ALPO
699 project. W. T. further acknowledges the Provincie West-Vlaanderen for his Chair in Advance
700 Materials, Research Foundation Flanders for his Odysseus fellowship (grant *G.0C60.13N*), and the
701 European Union's European Fund for Regional Development, Flanders Innovation &
702 Entrepreneurship and the Province of West-Flanders for financial support in the Accelerate³ project
703 (Interreg Vlaanderen-Nederland program). The authors would like to thank Prof. Dries Vandamme
704 for his contribution in the flocculation experiments.

705

706 **SUPPORTING INFORMATION**

- 707 • **Supplementary Table S1.** Conductometric titration results
- 708 • **Supplementary Table S2.** Dynamic viscosity at different shear rates (1.0 1/s 10.0 1/s and 100.0
709 1/s).
- 710 • **Supplementary Table S3.** Adhesion force values recorded between single *C. vulgaris* cells and
711 CNCs/chitosan coated surfaces.

- 712 • **Supplementary Table S4.** Adhesion force values and percentage of adhesions recorded between
713 single *C. vulgaris* cells and chitosan coated surface at pH 6 with increasing set point (applied force
714 during approach).
- 715 • **Supplementary Table S5.** Adhesion force values and percentage of adhesions recorded between
716 single *C. vulgaris* cells and chitosan coated surface at pH 8 with increasing set point (applied force
717 during approach).
- 718 • **Supplementary Table S6.** Young's modulus values recorded on *C. vulgaris* cells at pH 6 and pH 8.
719 Values were calculated from 80 nm indentation curves using the Hertz model.
- 720 • **Supplementary Figure S1.** Conductometric titration curve of chitosan with DD = $77.5 \pm 0.8\%$,
721 titrated with 5.75 mM NaOH. The replicas and chitosan samples provided by the Nha Trang
722 University have similar results and were not shown.
- 723 • **Supplementary Figure S2. Schematic representation of the three force spectroscopy methods**
724 **used.** a) CNCs (unmodified, PYR and MIM) or negatively charged beads functionalized cantilevers
725 are used to probe the interactions with cells immobilized on polyethylenimine coated glass
726 slides. b) A single *C. vulgaris* cell aspirated at the aperture of a FluidFM probe (4 μm) are used to
727 probe the interactions with CNCs-functionalized mica surfaces. c) AFM cantilevers functionalized
728 with a single *C. vulgaris* cells are used to probe the interactions with chitosan-functionalized
729 surfaces.
- 730 • **Supplementary Figure S3.** Scanning electron microscopy imaging of AFM cantilevers. a) AFM
731 cantilever with a single silica bead attached b) AFM cantilever with a silica bead functionalized
732 with an unmodified CNC particle c) AFM cantilever with a silica bead functionalized with a CNC-
733 MIM particle and d) AFM cantilever with a silica bead functionalized with a CNC-PYR particle.
- 734 • **Supplementary Figure S4.** Interactions between negative beads and CNC surfaces. a) Adhesion
735 force histogram between a COOH bead-functionalized cantilever and CNC-PYR immobilized on
736 mica at pH 8, b) corresponding rupture distance histogram c) Adhesion force histogram between
737 a COOH bead-functionalized cantilever and CNC-MIM at pH 8 d) corresponding rupture distance

738 histogram. Insets in b) and d) show representative force curves obtained. Data were recorded
739 using a set-point of 0.25 nN.

740

741 AUTHOR INFORMATION

742 Corresponding author: Cécile Formosa-Dague, formosa@insa-toulouse.fr

743 Toulouse Biotechnology Institute, INSA de Toulouse, 135 avenue de Rangeuil, 31077 Toulouse Cedex
744 4, France

745

746

747 AUTHOR CONTRIBUTIONS

748 The manuscript was written through contributions of all authors. All authors have given approval to
749 the final version of the manuscript. † I. D. and J. B. contributed equally to the work.

750

751 REFERENCES

- 752 (1) Pragma, N.; Pandey, K. K.; Sahoo, P. K. A Review on Harvesting, Oil Extraction and Biofuels
753 Production Technologies from Microalgae. *Renewable and Sustainable Energy Reviews* **2013**,
754 *24*, 159–171. <https://doi.org/10.1016/j.rser.2013.03.034>.
- 755 (2) Algae Bloom Again. *Nature* **2007**, *447* (7144), 520–521. <https://doi.org/10.1038/447520a>.
- 756 (3) Wijffels, R. H.; Barbosa, M. J. An Outlook on Microalgal Biofuels. *Science* **2010**, *329* (5993),
757 796–799. <https://doi.org/10.1126/science.1189003>.
- 758 (4) Mallick, N.; Mandal, S.; Singh, A. K.; Bishai, M.; Dash, A. Green Microalga *Chlorella Vulgaris* as
759 a Potential Feedstock for Biodiesel. *Journal of Chemical Technology & Biotechnology* **2012**, *87*
760 (1), 137–145. <https://doi.org/10.1002/jctb.2694>.
- 761 (5) Ziolkowska, J. R. Prospective Technologies, Feedstocks and Market Innovations for Ethanol
762 and Biodiesel Production in the US. *Biotechnology Reports* **2014**, *4*, 94–98.
763 <https://doi.org/10.1016/j.btre.2014.09.001>.
- 764 (6) Beijerinck, M. W. I. Kulturversuche Mit Zoochlorellen, Lichenengonidien Und Anderen
765 Niederen Algen. *Botanische Zeitung* **1890**, *48*, 729.
- 766 (7) Safi, C.; Zebib, B.; Merah, O.; Pontalier, P.-Y.; Vaca-Garcia, C. Morphology, Composition,
767 Production, Processing and Applications of *Chlorella Vulgaris*: A Review. *Renewable and*
768 *Sustainable Energy Reviews* **2014**, *35*, 265–278. <https://doi.org/10.1016/j.rser.2014.04.007>.
- 769 (8) Morimoto, T.; Nagatsu, A.; Murakami, N.; Sakakibara, J.; Tokuda, H.; Nishino, H.; Iwashima, A.
770 Anti-Tumour-Promoting Glyceroglycolipids from the Green Alga, *Chlorella Vulgaris*.
771 *Phytochemistry* **1995**, *40* (5), 1433–1437. [https://doi.org/10.1016/0031-9422\(95\)00458-J](https://doi.org/10.1016/0031-9422(95)00458-J).
- 772 (9) Justo, G. Z.; Silva, M. R.; Queiroz, M. L. S. Effects of the Green Algae *Chlorella Vulgaris* on the
773 Response of the Host Hematopoietic System to Intraperitoneal Ehrlich Ascites Tumor
774 Transplantation in Mice. *Immunopharmacology and Immunotoxicology* **2001**, *23* (1), 119–132.
775 <https://doi.org/10.1081/IPH-100102573>.

- 776 (10) Shen, X.-F.; Liu, J.-J.; Chauhan, A. S.; Hu, H.; Ma, L.-L.; Lam, P. K. S.; Zeng, R. J. Combining
777 Nitrogen Starvation with Sufficient Phosphorus Supply for Enhanced Biodiesel Productivity of
778 *Chlorella Vulgaris* Fed on Acetate. *Algal Research* **2016**, *17*, 261–267.
779 <https://doi.org/10.1016/j.algal.2016.05.018>.
- 780 (11) Shen, X.-F.; Qin, Q.-W.; Yan, S.-K.; Huang, J.-L.; Liu, K.; Zhou, S.-B. Biodiesel Production from
781 *Chlorella Vulgaris* under Nitrogen Starvation in Autotrophic, Heterotrophic, and Mixotrophic
782 Cultures. *J Appl Phycol* **2019**, *31* (3), 1589–1596. [https://doi.org/10.1007/s10811-019-01765-](https://doi.org/10.1007/s10811-019-01765-1)
783 [1](https://doi.org/10.1007/s10811-019-01765-1).
- 784 (12) Molina Grima, E.; Belarbi, E.-H.; Ación Fernández, F. G.; Robles Medina, A.; Chisti, Y. Recovery
785 of Microalgal Biomass and Metabolites: Process Options and Economics. *Biotechnology*
786 *Advances* **2003**, *20* (7), 491–515. [https://doi.org/10.1016/S0734-9750\(02\)00050-2](https://doi.org/10.1016/S0734-9750(02)00050-2).
- 787 (13) Singh, G.; Patidar, S. K. Microalgae Harvesting Techniques: A Review. *Journal of Environmental*
788 *Management* **2018**, *217*, 499–508. <https://doi.org/10.1016/j.jenvman.2018.04.010>.
- 789 (14) Lardon, L.; Hélias, A.; Sialve, B.; Steyer, J.-P.; Bernard, O. Life-Cycle Assessment of Biodiesel
790 Production from Microalgae. *Environ. Sci. Technol.* **2009**, *43* (17), 6475–6481.
791 <https://doi.org/10.1021/es900705j>.
- 792 (15) Shimako, A. H.; Tiruta-Barna, L.; Pigné, Y.; Benetto, E.; Navarrete Gutiérrez, T.; Guiraud, P.;
793 Ahmadi, A. Environmental Assessment of Bioenergy Production from Microalgae Based
794 Systems. *Journal of Cleaner Production* **2016**, *139*, 51–60.
795 <https://doi.org/10.1016/j.jclepro.2016.08.003>.
- 796 (16) Kadir, W. N. A.; Lam, M. K.; Uemura, Y.; Lim, J. W.; Lee, K. T. Harvesting and Pre-Treatment of
797 Microalgae Cultivated in Wastewater for Biodiesel Production: A Review. *Energy Conversion*
798 *and Management* **2018**, *171*, 1416–1429. <https://doi.org/10.1016/j.enconman.2018.06.074>.
- 799 (17) Vandamme, D.; Foubert, I.; Muylaert, K. Flocculation as a Low-Cost Method for Harvesting
800 Microalgae for Bulk Biomass Production. *Trends in Biotechnology* **2013**, *31* (4), 233–239.
801 <https://doi.org/10.1016/j.tibtech.2012.12.005>.
- 802 (18) Vandamme, D.; Foubert, I.; Muylaert, K. Flocculation as a Low-Cost Method for Harvesting
803 Microalgae for Bulk Biomass Production. *Trends in Biotechnology* **2013**, *31* (4), 233–239.
804 <https://doi.org/10.1016/j.tibtech.2012.12.005>.
- 805 (19) Pugazhendhi, A.; Shobana, S.; Bakonyi, P.; Nemestóthy, N.; Xia, A.; Banu J, R.; Kumar, G. A
806 Review on Chemical Mechanism of Microalgae Flocculation via Polymers. *Biotechnology*
807 *Reports* **2019**, *21*, e00302. <https://doi.org/10.1016/j.btre.2018.e00302>.
- 808 (20) Renault, F.; Sancey, B.; Badot, P.-M.; Crini, G. Chitosan for Coagulation/Flocculation Processes
809 – An Eco-Friendly Approach. *European Polymer Journal* **2009**, *45* (5), 1337–1348.
810 <https://doi.org/10.1016/j.eurpolymj.2008.12.027>.
- 811 (21) Chen, G.; Zhao, L.; Qi, Y.; Cui, Y.-L. Chitosan and Its Derivatives Applied in Harvesting
812 Microalgae for Biodiesel Production: An Outlook
813 <https://www.hindawi.com/journals/jnm/2014/217537/> (accessed Feb 3, 2020).
814 <https://doi.org/10.1155/2014/217537>.
- 815 (22) Ahmad, A. L.; Mat Yasin, N. H.; Derek, C. J. C.; Lim, J. K. Optimization of Microalgae
816 Coagulation Process Using Chitosan. *Chemical Engineering Journal* **2011**, *173* (3), 879–882.
817 <https://doi.org/10.1016/j.cej.2011.07.070>.
- 818 (23) Ritthidej, G. C. Chapter 3 - Nasal Delivery of Peptides and Proteins with Chitosan and Related
819 Mucoadhesive Polymers. In *Peptide and Protein Delivery*; Van Der Walle, C., Ed.; Academic
820 Press: Boston, 2011; pp 47–68. <https://doi.org/10.1016/B978-0-12-384935-9.10003-3>.
- 821 (24) Bilanovic, D.; Shelef, G.; Sukenik, A. Flocculation of Microalgae with Cationic Polymers —
822 Effects of Medium Salinity. *Biomass* **1988**, *17* (1), 65–76. [https://doi.org/10.1016/0144-](https://doi.org/10.1016/0144-4565(88)90071-6)
823 [4565\(88\)90071-6](https://doi.org/10.1016/0144-4565(88)90071-6).
- 824 (25) Rashid, N.; Rehman, S. U.; Han, J.-I. Rapid Harvesting of Freshwater Microalgae Using
825 Chitosan. *Process Biochemistry* **2013**, *48* (7), 1107–1110.
826 <https://doi.org/10.1016/j.procbio.2013.04.018>.

- 827 (26) Low, Y. J.; Lau, S. W. Effective Flocculation of *Chlorella Vulgaris* Using Chitosan with Zeta
828 Potential Measurement. *IOP Conf. Ser.: Mater. Sci. Eng.* **2017**, *206*, 012073.
829 <https://doi.org/10.1088/1757-899X/206/1/012073>.
- 830 (27) Matho, C.; Schwarzenberger, K.; Eckert, K.; Keshavarzi, B.; Walther, T.; Steingroewer, J.;
831 Krujatz, F. Bio-Compatible Flotation of *Chlorella Vulgaris*: Study of Zeta Potential and Flotation
832 Efficiency. *Algal Research* **2019**, *44*, 101705. <https://doi.org/10.1016/j.algal.2019.101705>.
- 833 (28) Garzon-Sanabria, A. J.; Ramirez-Caballero, S. S.; Moss, F. E. P.; Nikolov, Z. L. Effect of Algogenic
834 Organic Matter (AOM) and Sodium Chloride on *Nannochloropsis Salina* Flocculation Efficiency.
835 *Bioresource Technology* **2013**, *143*, 231–237. <https://doi.org/10.1016/j.biortech.2013.05.125>.
- 836 (29) Farid, M. S.; Shariati, A.; Badakhshan, A.; Anvaripour, B. Using Nano-Chitosan for Harvesting
837 Microalga *Nannochloropsis Sp.* *Bioresource Technology* **2013**, *131*, 555–559.
838 <https://doi.org/10.1016/j.biortech.2013.01.058>.
- 839 (30) Faridi, M. A.; Ramachandraiah, H.; Banerjee, I.; Ardabili, S.; Zelenin, S.; Russom, A. Elasto-
840 Inertial Microfluidics for Bacteria Separation from Whole Blood for Sepsis Diagnostics. *Journal*
841 *of Nanobiotechnology* **2017**, *15* (1). <https://doi.org/10.1186/s12951-016-0235-4>.
- 842 (31) Blockx, J.; Verfaillie, A.; Thielemans, W.; Muylaert, K. Unravelling the Mechanism of Chitosan-
843 Driven Flocculation of Microalgae in Seawater as a Function of PH. *ACS Sustainable Chem. Eng.*
844 **2018**, *6* (9), 11273–11279. <https://doi.org/10.1021/acssuschemeng.7b04802>.
- 845 (32) Cheng, Y.-S.; Zheng, Y.; Labavitch, J. M.; VanderGheynst, J. S. The Impact of Cell Wall
846 Carbohydrate Composition on the Chitosan Flocculation of *Chlorella*. *Process Biochemistry*
847 **2011**, *46* (10), 1927–1933. <https://doi.org/10.1016/j.procbio.2011.06.021>.
- 848 (33) Binnig, G.; Quate, C. F.; Gerber, C. Atomic Force Microscope. *Physical Review Letters* **1986**, *56*
849 (9), 930–934.
- 850 (34) Formosa-Dague, C.; Gernigon, V.; Castelain, M.; Daboussi, F.; Guiraud, P. Towards a Better
851 Understanding of the Flocculation/Flotation Mechanism of the Marine Microalgae
852 *Phaeodactylum Tricornutum* under Increased PH Using Atomic Force Microscopy. *Algal*
853 *Research* **2018**, *33*, 369–378. <https://doi.org/10.1016/j.algal.2018.06.010>.
- 854 (35) Besson, A.; Formosa-Dague, C.; Guiraud, P. Flocculation-Flotation Harvesting Mechanism of
855 *Dunaliella Salina*: From Nanoscale Interpretation to Industrial Optimization. *Water Research*
856 **2019**, *155*, 352–361. <https://doi.org/10.1016/j.watres.2019.02.043>.
- 857 (36) Vergnes, J. B.; Gernigon, V.; Guiraud, P.; Formosa-Dague, C. Bicarbonate Concentration
858 Induces Production of Exopolysaccharides by *Arthrospira Platensis* That Mediate
859 Bioflocculation and Enhance Flotation Harvesting Efficiency. *ACS Sustainable Chem. Eng.* **2019**,
860 *7* (16), 13796–13804. <https://doi.org/10.1021/acssuschemeng.9b01591>.
- 861 (37) Blockx, J.; Verfaillie, A.; Eyley, S.; Deschaume, O.; Bartic, C.; Muylaert, K.; Thielemans, W.
862 Cationic Cellulose Nanocrystals for Flocculation of Microalgae: Effect of Degree of Substitution
863 and Crystallinity. *ACS Appl. Nano Mater.* **2019**, *2* (6), 3394–3403.
864 <https://doi.org/10.1021/acsanm.9b00315>.
- 865 (38) Chen, L.; Chen, D.; Wu, C. A New Approach for the Flocculation Mechanism of Chitosan.
866 *Journal of Polymers and the Environment* **2003**, *11* (3), 87–92.
867 <https://doi.org/10.1023/A:1024656813244>.
- 868 (39) Demir, I.; Besson, A.; Guiraud, P.; Formosa-Dague, C. Towards a Better Understanding of
869 Microalgae Natural Flocculation Mechanisms to Enhance Flotation Harvesting Efficiency.
870 *Water Sci Technol* **2020**. <https://doi.org/10.2166/wst.2020.177>.
- 871 (40) Verfaillie, A.; Blockx, J.; Praveenkumar, R.; Thielemans, W.; Muylaert, K. Harvesting of Marine
872 Microalgae Using Cationic Cellulose Nanocrystals. *Carbohydrate Polymers* **2020**, *240*, 116165.
873 <https://doi.org/10.1016/j.carbpol.2020.116165>.
- 874 (41) Alsteens, D.; Beaussart, A.; Derclaye, S.; El-Kirat-Chatel, S.; Park, H. R.; Lipke, P. N.; Dufrêne, Y.
875 F. Single-Cell Force Spectroscopy of Als-Mediated Fungal Adhesion. *Anal. Methods* **2013**, *5*
876 (15), 3657–3662. <https://doi.org/10.1039/C3AY40473K>.

- 877 (42) Yao, H.-B.; Fang, H.-Y.; Tan, Z.-H.; Wu, L.-H.; Yu, S.-H. Biologically Inspired, Strong, Transparent,
878 and Functional Layered Organic–Inorganic Hybrid Films. *Angewandte Chemie International*
879 *Edition* **2010**, *49* (12), 2140–2145. <https://doi.org/10.1002/anie.200906920>.
- 880 (43) Carapeto, A. P.; Ferrara, A. M.; Rego, A. M. B. do. Chitosan Thin Films on Glass and Silicon
881 Substrates. *Microscopy and Microanalysis* **2015**, *21* (S5), 13–14.
882 <https://doi.org/10.1017/S1431927615013872>.
- 883 (44) Formosa, C.; Grare, M.; Jauvert, E.; Coutable, A.; Regnouf-de-Vains, J. B.; Mourer, M.; Duval, R.
884 E.; Dague, E. Nanoscale Analysis of the Effects of Antibiotics and CX1 on a Pseudomonas
885 Aeruginosa Multidrug-Resistant Strain. *Sci. Rep.* **2012**, *2*. <https://doi.org/10.1038/srep00575>.
- 886 (45) Formosa-Dague, C.; Speziale, P.; Foster, T. J.; Geoghegan, J. A.; Dufrêne, Y. F. Zinc-Dependent
887 Mechanical Properties of Staphylococcus Aureus Biofilm-Forming Surface Protein SasG. *PNAS*
888 **2016**, *113* (2), 410–415. <https://doi.org/10.1073/pnas.1519265113>.
- 889 (46) Formosa-Dague, C.; Feuillie, C.; Beaussart, A.; Derclaye, S.; Kucharíková, S.; Lasa, I.; Van Dijck,
890 P.; Dufrêne, Y. F. Sticky Matrix: Adhesion Mechanism of the Staphylococcal Polysaccharide
891 Intercellular Adhesin. *ACS Nano* **2016**, *10* (3), 3443–3452.
892 <https://doi.org/10.1021/acs.nano.5b07515>.
- 893 (47) Higgins, M. J.; Molino, P.; Mulvaney, P.; Wetherbee, R. The Structure and Nanomechanical
894 Properties of the Adhesive Mucilage That Mediates Diatom-Substratum Adhesion and
895 Motility1. *Journal of Phycology* **2003**, *39* (6), 1181–1193. <https://doi.org/10.1111/j.0022-3646.2003.03-027.x>.
- 897 (48) Myllytie, P.; Salmi, J.; Laine, J. THE INFLUENCE OF PH ON THE ADSORPTION AND INTERACTION
898 OF CHITOSAN WITH CELLULOSE. *BioResources* **2009**, *4* (4), 1647–1662.
- 899 (49) Simsek-Ege, F. A.; Bond, G. M.; Stringer, J. Polyelectrolyte Complex Formation between
900 Alginate and Chitosan as a Function of PH. *Journal of Applied Polymer Science* **2003**, *88* (2),
901 346–351. <https://doi.org/10.1002/app.11989>.
- 902 (50) Barany, S.; Szepesszentgyörgyi, A. Flocculation of Cellular Suspensions by Polyelectrolytes.
903 *Advances in Colloid and Interface Science* **2004**, *111* (1), 117–129.
904 <https://doi.org/10.1016/j.cis.2004.07.003>.
- 905 (51) Boonsongrit, Y.; Mitrevej, A.; Mueller, B. W. Chitosan Drug Binding by Ionic Interaction.
906 *European Journal of Pharmaceutics and Biopharmaceutics* **2006**, *62* (3), 267–274.
907 <https://doi.org/10.1016/j.ejpb.2005.09.002>.
- 908 (52) Hertz, H. Ueber Die Berührung Fester Elastischer Körper. *Journal für die reine und angewandte*
909 *mathematik* **1881**, 156–171.
- 910 (53) Formosa, C.; Schiavone, M.; Martin-Yken, H.; François, J. M.; Duval, R. E.; Dague, E. Nanoscale
911 Effects of Caspofungin against Two Yeast Species, Saccharomyces Cerevisiae and Candida
912 Albicans. *Antimicrob. Agents Chemother.* **2013**, *57* (8), 3498–3506.
913 <https://doi.org/10.1128/AAC.00105-13>.
- 914 (54) Guillard, R. R. L.; Lorenzen, C. J. Yellow-Green Algae with Chlorophyllide C2. *Journal of*
915 *Phycology* **1972**, *8* (1), 10–14.
- 916 (55) Hutter, J. L.; Bechhoefer, J. Calibration of Atomic-Force Microscope Tips. *Review of Scientific*
917 *Instruments* **1993**, *64* (7), 1868–1873.
- 918 (56) Francius, G.; Tesson, B.; Dague, E.; Martin-Jézéquel, V.; Dufrêne, Y. F. Nanostructure and
919 Nanomechanics of Live Phaeodactylum Tricornutum Morphotypes. *Environ. Microbiol.* **2008**,
920 *10* (5), 1344–1356. <https://doi.org/10.1111/j.1462-2920.2007.01551.x>.
- 921